The yeast pantothenate kinase Cab1 is a master regulator of sterol metabolism and of susceptibility to ergosterol biosynthesis inhibitors

Received for publication, June 14, 2019, and in revised form, August 12, 2019 Published, Papers in Press, August 13, 2019, DOI 10.1074/jbc.RA119.009791

Joy E. Chiu[‡], Jose Thekkiniath[‡], Sameet Mehta[§], Christoph Müller[¶], Franz Bracher[¶], and Choukri Ben Mamoun[‡1]

From the [‡]Section of Infectious Diseases, Department of Internal Medicine and [§]Department of Genetics, Yale University School of Medicine, New Haven, Connecticut 06520 and [¶]Department of Pharmacy–Center for Drug Research, Ludwig Maximilians University Munich, Butenandstrasse 5-13, 81377 Munich, Germany

Edited by George M. Carman

In fungi, ergosterol is an essential component of the plasma membrane. Its biosynthesis from acetyl-CoA is the primary target of the most commonly used antifungal drugs. Here, we show that the pantothenate kinase Cab1p, which catalyzes the first step in the metabolism of pantothenic acid for CoA biosynthesis in budding yeast (*Saccharomyces cerevisiae*), significantly regulates the levels of sterol intermediates and the activities of ergosterol biosynthesis-targeting antifungals. Using genetic and pharmacological analyses, we show that altered pantothenate utilization dramatically alters the susceptibility of yeast cells to ergosterol biosynthesis inhibitors. Genome-wide transcription and MS-based analyses revealed that this regulation is mediated by changes both in the expression of ergosterol biosynthesis genes and in the levels of sterol intermediates. Consistent with these findings, drug interaction experiments indicated that inhibition of pantothenic acid utilization synergizes with the activity of the ergosterol molecule–targeting antifungal amphotericin B and antagonizes that of the ergosterol pathway–targeting antifungal drug terbinafine. Our finding that CoA metabolism controls ergosterol biosynthesis and susceptibility to antifungals could set the stage for the development of new strategies to manage fungal infections and to modulate the potency of current drugs against drug-sensitive and -resistant fungal pathogens.

Fungal diseases are a major global health problem and are particularly threatening as opportunistic infections in immunosuppressed individuals such as AIDS and cancer patients (1, 2). Despite major advances in understanding the biology of fungi and in antifungal drug discovery, fungal infections continue to cause significant mortality and morbidity worldwide (3). Commonly used antifungal drugs include azoles, echinocandins, polyenes, and allylamines (4). However, due to widespread resistance to some of these drugs and their lack of efficacy against a diverse array of pathogens such as *Candida albicans*, *Candida auris*, and *Aspergillus fumigatus*, both new drugs and alternative strategies to modulate the efficacy and safety of current drugs and reverse resistance are urgently needed.

In all living organisms, coenzyme A (CoA) plays a fundamental role in cellular metabolism. Fig. 1 shows a simplified schematic of metabolic pathways for CoA biosynthesis in yeast, whereas Fig. 2 shows more comprehensive detail. The unique chemical structure of CoA, with a reactive thiol group and a nucleotide moiety, allows it to serve as a cofactor in critical biochemical and regulatory functions through activation of carboxylic acids and production of thioester derivatives (5). In the yeast *Saccharomyces cerevisiae*, CoA is synthesized from vitamin B_5 (pantothenic acid) either imported into the cell via the Fen2p pantothenate transporter or produced *de novo* from the ligation of β-alanine and pantoate by the pantothenate synthase Pan6p (6, 7) (Figs. 1 and 2). Pantothenic acid utilization is absolutely essential for yeast survival as a double mutant lacking both the *FEN2* and *PAN6* genes is inviable (8). The first step in pantothenate utilization is its phosphorylation by the pantothenate kinase Cab1p, encoded by a single-copy gene, *CAB1* (8). This gene is required for yeast viability as deletion of *CAB1* results in cell death. A mutant, *cab1^{ts}*, which produces a kinase enzyme with glycine 351 substituted to serine, was found to be viable at 30 °C but is completely inviable at 37 °C (8). Biochemical assays using purified WT and mutated Cab1p enzymes showed that the G351S substitution results in ~94% loss of enzyme activity (9). Recent studies showed that the pantothenate analog α-PanAm[2] inhibits yeast growth in a pantothenic acid dose-dependent manner (9). The MIC_{50} of the compound was found to be ~4 times higher in medium supplemented with 1 μM pantothenic acid (MIC_{50} ~ 7.6 μg/ml) compared with medium with 100 nM pantothenic acid (MIC_{50} ~ 1.9 μg/ml) (9). *In vitro* pantothenate phosphorylation assays and MS analysis showed that α-PanAm is also phosphorylated by Cab1p and acts as a competitor of pantothenic acid at the enzyme catalytic

Joy E. Chiu, Jose Thekkiniath, and Choukri Ben Mamoun are listed on a patent application for targeting pantothenate kinase (PanK) activity for development of antifungal drugs. Choukri Ben Mamoun is the founder of a company that aims to develop such drugs.

This article contains Figs. S1 and S2.

[1] To whom correspondence should be addressed: Section of Infectious Diseases, Dept. of Internal Medicine, Yale University School of Medicine, Winchester Bldg. WWW403D, 15 York St., New Haven, CT 06520. Tel.: 203-737-1972; E-mail: choukri.benmamoun@yale.edu.

[2] The abbreviations used are: α-PanAm, alpha-methyl-N-phenethyl-pantothenamide; MIC_{50}, minimum inhibitory concentration; ERG, ergosterol biosynthesis gene; ts, thermosensitive; T-MAS, testis meiosis-activating sterol; PA, pantothenate; FIC, fractional inhibitory concentration; FPKM, fragments per kilobase of transcript per million mapped reads.

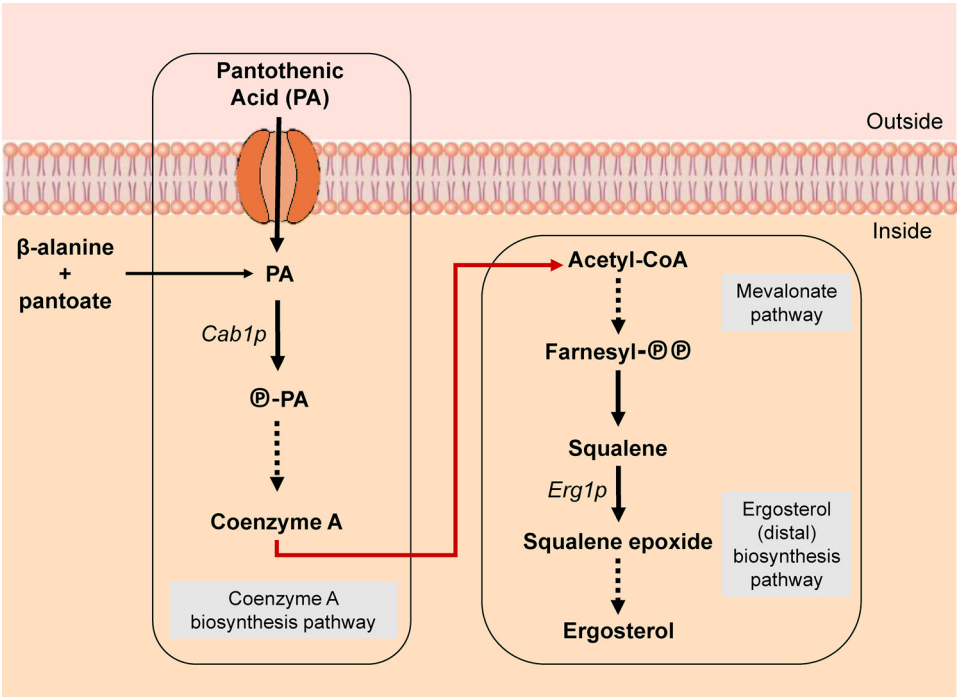

Figure 1. Simplified CoA and ergosterol biosynthesis pathways in yeast. Shown is a schematic representation of key intermediates in the metabolic pathways for CoA and ergosterol biosynthesis in the yeast *S. cerevisiae*. The CoA biosynthesis and ergosterol biosynthesis pathways are each *boxed* to demonstrate their separate treatment and lack of link in the current literature. The *red arrow* represents our novel conclusions, demonstrating the regulation that the CoA biosynthesis pathway exerts over the ergosterol biosynthesis pathway. *Solid arrows* represent single enzymatic steps between intermediates. *Dashed arrows* indicate multiple steps between intermediates. Further detailed enzymatic steps involved in these processes are shown in Fig. 2.

site (9). α-PanAm has also been shown to act on downstream steps in CoA biosynthesis and to reduce cellular CoA levels (10). In fungi, acetylation of CoA by acetyl-CoA synthetases generates acetyl-CoA, a key node in multiple metabolic and cellular processes, including the synthesis of ergosterol, an essential component of the plasma and mitochondrial membranes (Figs. 1 and 2). Ergosterol serves fundamental cellular functions such as maintenance of membrane fluidity, permeability to nutrients and solutes, and response to environmental stresses (11). The ergosterol biosynthesis pathway from acetyl-CoA involves 24 known Erg enzymes and can be divided into two main subpathways, the mevalonate route and the squalene-to-ergosterol route (also known as the distal ergosterol biosynthesis route) (11) (Figs. 1 and 2). The mevalonate route produces farnesyl pyrophosphate, which in the ERG biosynthesis pathway serves as an intermediate in the synthesis of the triterpene (C_{30}) squalene; whereas the distal route produces ergosterol from squalene and is the main target of allylamines, azoles, morpholines, and polyenes (Figs. 1 and 2). Some of the ergosterol biosynthesis enzymes in the distal route can also catalyze alternative reactions to produce nonphysiological sterol intermediates, some of which have been shown to inhibit fungal growth (11). This ability becomes relevant in cases of inhibition of enzymes in the pathway that causes accumulation of toxic steroidal substrates, which can then be metabolized through these alternative reactions. One of the first rate-limiting steps in the distal pathway is squalene oxygenation to form squalene epoxide catalyzed by squalene epoxidase, Erg1p. This enzyme is the target of the major allylamine-type antifungal drug terbinafine (12). Inhibition of Erg1p by terbinafine results in accumulation of squalene in the cell, which impairs fungal membrane function (13, 14).

Although ergosterol metabolism and inhibition have been studied extensively, the effect of pantothenic acid utilization and CoA metabolism on these processes remains completely unknown. Here, we report the first evidence for an important role of the CoA biosynthesis pathway and pantothenate phosphorylation in the regulation of ergosterol metabolism and yeast sensitivity to antifungals. We show that modulation of Cab1p activity results in altered sterol levels and dramatic changes in yeast susceptibility to drugs that target late enzymes in ergosterol biosynthesis.

Results

Reduced pantothenate phosphorylation results in altered yeast susceptibility to antifungals

Previous studies have shown that yeast cells altered in the uptake of pantothenic acid through the Fen2p transporter display reduced susceptibility to fenpropimorph, a morpholine-type antifungal, which targets the enzymes sterol C14-reductase (*ERG24*) and sterol C8-isomerase (*ERG2*) in the ergosterol biosynthesis pathway (6, 7). This led us to investigate whether pantothenic acid utilization regulates ergosterol biosynthesis and yeast sensitivity to antifungals. The first step in pantothenic acid utilization is catalyzed by the pantothenate kinase Cab1p. In yeast, this step is essential for cell viability as knockout of the *CAB1* gene results in cell death. Substitution of glycine 351 to serine in Cab1p results in a thermosensitive (ts) phenotype in which the yeast cells are unable to grow at 37 °C (8, 9) (Fig. 3*A*).

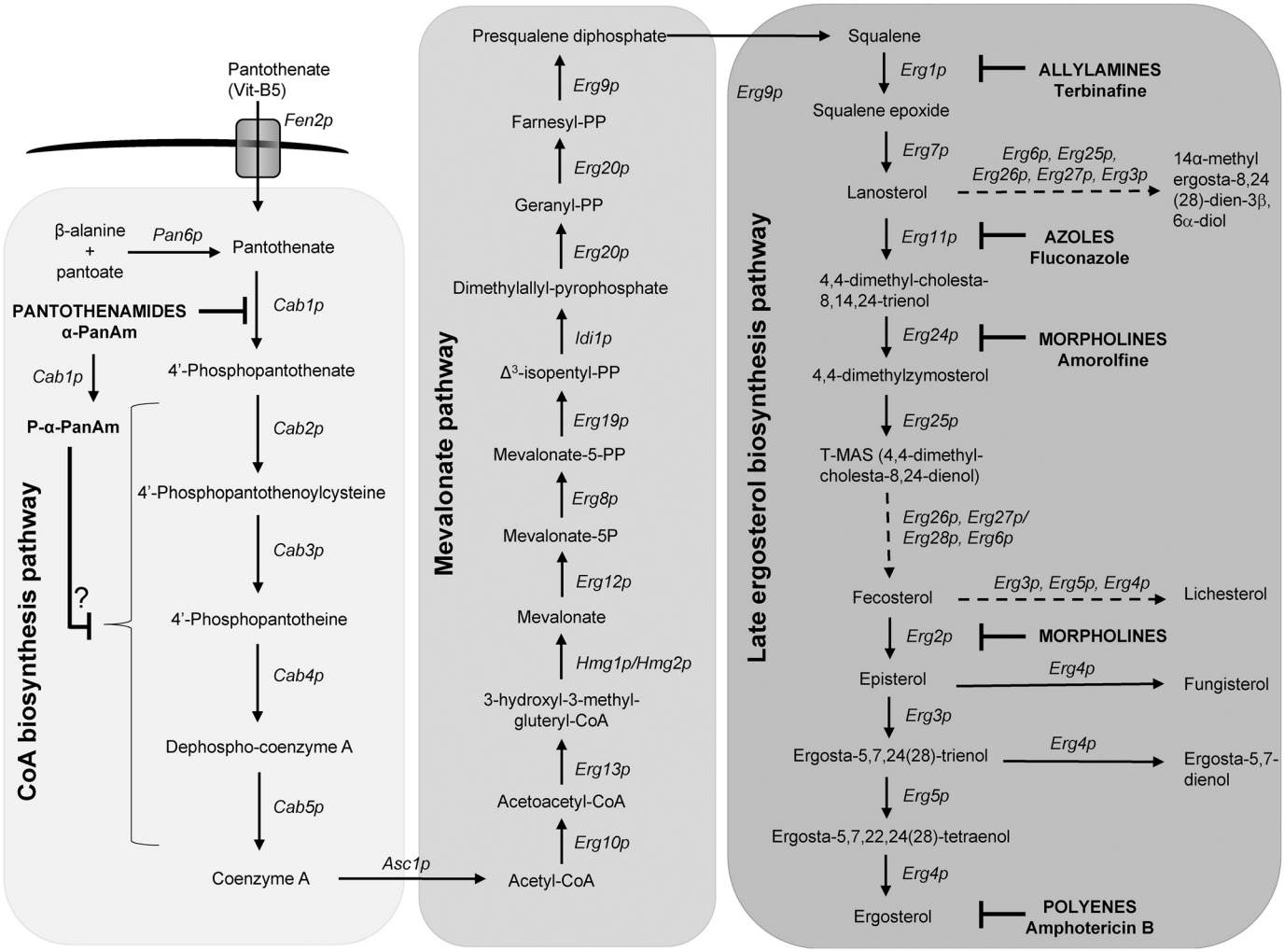

Figure 2. Detailed metabolic pathway from pantothenate to ergosterol. The pathway is divided into three subpathways: the CoA biosynthesis pathway from pantothenate (*first box*), the mevalonate pathway (*second box*), and the distal ergosterol biosynthetic pathway (*third box*). *Solid arrows* represent single enzymatic steps. *Dashed arrows* indicate multiple steps, catalyzed by the proteins in the order they are listed, from one intermediate to the next. Drug classes, individual drugs, and their site of action are shown in *bold*. *Vit*, vitamin; *AAT*, amino acid transporter; P-α-PanAm, phosphorylated α-PanAm.

Biochemical analyses showed that the activity of the mutant Cab1^{G351S}p pantothenate kinase is only ~7% that of the WT at 30 °C (Fig. 3*B*). The availability of the yeast *cab1^{ts}* mutant strain made it possible to assess the effect of altered pantothenate kinase activity on yeast susceptibility to antifungals at 30 °C. As shown in Fig. 3*C*, whereas the growth of the WT was inhibited by amorolfine, fluconazole, and terbinafine, the growth of the *cab1^{ts}* mutant was not affected by these drugs. Conversely, with a sublethal dose of amphotericin B (1 μg/ml), the growth of the WT strain was only slightly inhibited, whereas that of the *cab1^{ts}* mutant was reduced dramatically in the presence of the compound (Fig. 3*C*). MIC_{50} values for these drugs against the two yeast strains were obtained for cell growth in liquid YPD medium (2% Bacto Peptone, 2% D-(+)-glucose, and 1% yeast extract). According to these values, the WT strain was about 10× more susceptible to amorolfine, about 30× more susceptible to fluconazole, and about 150× more susceptible to terbinafine than the *cab1^{ts}* strain. Conversely, *cab1^{ts}* cells were about 5× more susceptible to amphotericin B than WT cells (Fig. 3*D*).

Inhibition of pantothenate utilization results in reduced susceptibility to terbinafine

To further investigate the link between pantothenate utilization and antifungal susceptibility, we examined the effect of inhibition of Cab1p activity on yeast susceptibility to terbinafine. Consistent with its defect in pantothenic acid utilization, the growth of the *cab1^{ts}* mutant under permissive conditions was ameliorated with pantothenic acid supplementation as the times to mid-log phase were 48, 36, and 28 h for cells grown in media supplemented with 1, 10, and 100 μM pantothenic acid, respectively (Fig. 4, *B*, *D*, and *F*). Comparatively, the growth of the WT strain was not significantly altered by increasing concentrations of pantothenic acid as the times to mid-log phase were ~26, 24, and 24 h at 1, 10, and 100 μM pantothenic acid, respectively (Fig. 4, *A*, *C*, and *E*). Interestingly, whereas the growth of the WT was dramatically decreased in media supplemented with 1 μM pantothenic acid in the presence of terbinafine (relative time to mid-log phase of 1.8 in the presence *versus* absence of the drug), the growth of the *cab1^{ts}* mutant was only moderately affected by the drug (relative time to mid-log

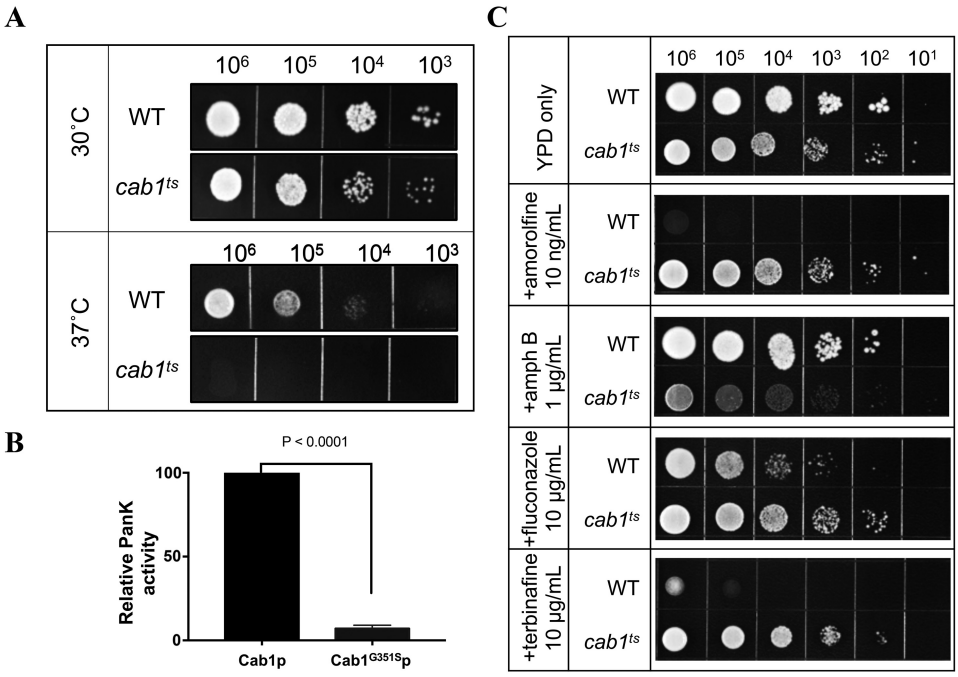

D

	WT MIC_{50}	*cab1ts* MIC_{50}	*cab1ts* MIC_{50} / WT MIC_{50}
Amorolfine (ng/mL)	0.091 ± 0.016	0.881 ± 0.269	9.68x
Amphotericin B (µg/mL)	1.170 ± 0.044	0.235 ± 0.162	0.20x
Fluconazole (µg/mL)	11.295 ± 0.262	349.15 ± 47.588	30.91x
Terbinafine (µg/mL)	1.469 ± 0.278	227.4 ± 146.654	154.80x

Figure 3. Reduced pantothenate kinase activity results in altered sensitivity to antifungals. *A*, WT and *cab1ts* cells were spotted on YPD agar plates (with grid) at cell densities ranging between 10^3 and 10^6 cells and incubated at 30 and 37 °C. Images were collected 48 h postinoculation. *B*, pantothenate kinase (*PanK*) activity of WT Cab1p and Cab1^{G351S}p measured using the Kinase-Glo assay. *, *p* value < 0.0001. *C*, WT and *cab1ts* cells were spotted on YPD agar plates at limiting dilution, with cell densities ranging between 10^6 and 10^1 cells/spot. All plates were incubated at 30 °C in the absence or presence of 10 ng/ml amorolfine, 1 µg/ml amphotericin B, 10 µg/ml fluconazole, or 10 µg/ml terbinafine. All images were collected 48 h postinoculation. *D*, MIC_{50} values of compounds against WT and *cab1ts* cells grown in liquid YPD medium, as calculated by the Clinical and Laboratory Standards Institute standard method M27-A3. The *final column* compares the -fold change in MIC_{50} for *cab1ts* over WT. *Error bars* represent SD.

phase of 1.1 in the presence *versus* absence of the drug) (Fig. 4*G*). Addition of pantothenic acid to the culture medium at 10 or 100 µM resulted in higher sensitivity of both the WT (relative time to mid-log phase of 2.1 and 2.3 in the presence of 10 and 100 µM, respectively) and the *cab1ts* mutant (relative time to mid-log phase of 1.4 and 1.6 in the presence of 10 and 100 µM, respectively) to terbinafine (Fig. 4*G*).

Because reduced activity of Cab1p in *cab1ts* cells correlated with reduced susceptibility to terbinafine, we reasoned that chemical inhibition of Cab1p activity and/or CoA biosynthesis in the WT could also result in reduced susceptibility to the drug. We therefore examined the susceptibility of the WT to terbinafine in the presence of the pantothenamide α-PanAm (9). As shown in the isobologram in Fig. 4*H*, terbinafine and α-PanAm displayed a typical drug–drug antagonism pattern in the WT, suggesting that inhibition of pantothenate utilization and CoA biosynthesis results in reduced susceptibility to terbinafine.

Inhibition of pantothenate utilization results in enhanced susceptibility to amphotericin B

Our studies also showed that the sensitivity of WT *S. cerevisiae* to amphotericin B depended on pantothenic acid availability. Whereas the growth rate of the WT strain was only moderately inhibited by 1 µg/ml amphotericin B in media supplemented with 100 µM pantothenic acid, it was significantly affected in media containing 1 µM pantothenic acid (relative time to mid-log phase of 2.1 in the presence *versus* absence of the drug) (Fig. 5, *A*, *C*, *E*, and *G*). Interestingly, the *cab1ts* mutant showed a much higher sensitivity to amphotericin B compared with the WT (Fig. 5, *B*, *D*, *F*, and *G*), indicating that reduced pantothenate kinase activity leads to increased sensitivity to this drug. Consistent with this phenotype, drug–drug interactions showed synergistic effects between amphotericin B and α-PanAm (Fig. 5*H*).

Inhibition of Cab1p activity results in reduced squalene and lanosterol levels

To investigate the mechanism by which modulation of Cab1p activity alters yeast susceptibility to antifungals, we compared the levels of ergosterol, squalene, and other predominant sterol precursors by gas chromatography–mass spectrometry (GC-MS) between WT and *cab1ts* strains under permissive conditions. Ergosterol comprised the largest percentage of total sterols in both WT and *cab1ts* cells followed by the open-chain sterol precursor squalene. All other sterols each comprised no

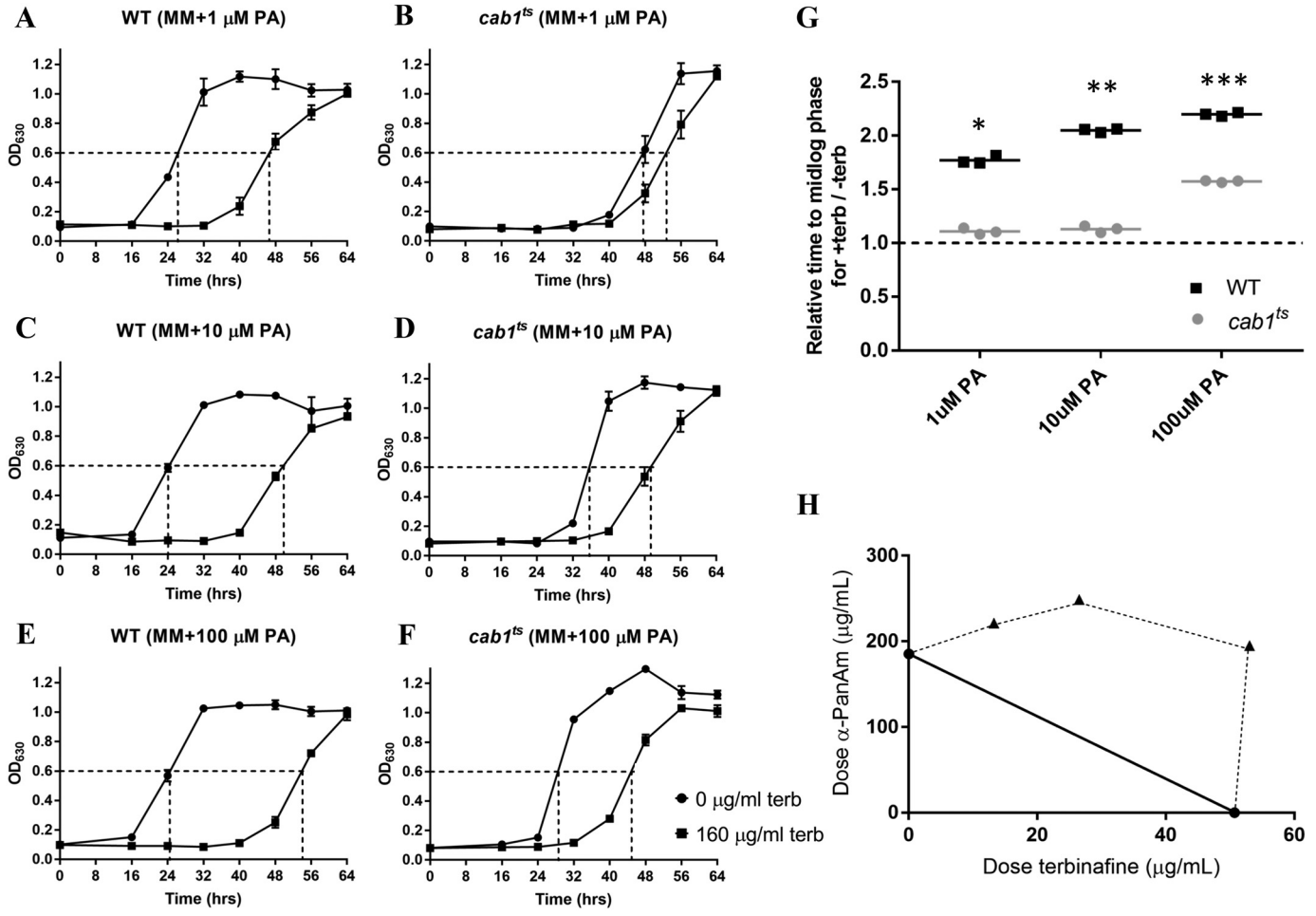

Figure 4. Relationship between pantothenate utilization and yeast susceptibility to terbinafine. *A–F*, growth curves of WT and *cab1*^{ts} cells without or with 160 μg/ml terbinafine (*terb*) in liquid minimal medium supplemented with varying concentrations of pantothenic acid. *MM*, minimal medium. *G*, relative times for treated WT and *cab1*^{ts} cells to reach mid-log phase compared with untreated cells, calculated from *A*. Time for untreated cells to grow to mid-log was normalized to 1 and is represented by the *dashed line*. Comparing the WT with *cab1*^{ts} growth at each PA concentration provides significant results. *, *p* value < 0.0001; **, *p* value < 0.0001; ***, *p* value < 0.0001. *H*, isobologram of the interaction between terbinafine and the pantothenate analog α-PanAm ($n = 2$). The *solid line* represents the theoretical curve of an additive effect. Data above the *solid line* (*dashed* curve) show antagonism between the two compounds. *Error bars* represent SD.

more than ~10% of total sterols (Fig. 6*A*). As shown in Fig. 6*B*, reduced pantothenate phosphorylation in the *cab1*^{ts} mutant resulted in a significant reduction in the levels of squalene and lanosterol and a significant increase in ergosterol content. Consistent with these findings, supplementation of the growth medium of WT cells with 100 μg/ml squalene had only a slight effect on cell growth (mid-log phase reached at 28 h in the absence of squalene *versus* 34 h in the presence of squalene), whereas in the presence of terbinafine, the growth of WT cells was dramatically reduced (mid-log phase reached at 47 h in the absence of squalene *versus* 61 h in the presence of squalene) (Fig. 6, *C* and *D*).

To determine whether the reduced level of squalene seen in the *cab1*^{ts} mutant could also be due to changes in the transcription of the *ERG1* gene or other genes in the ERG biosynthetic pathway, we performed RNA-Seq analysis on WT and *cab1*^{ts} strains grown under permissive conditions (minimal medium supplemented with 100 μM pantothenic acid). Two high-quality mRNA samples were selected for RNA-Seq analysis from two independent replicates, and the expression of the CoA biosynthesis genes (*CAB1–5*), ergosterol biosynthesis genes (20 *ERG* genes), and the transcriptional factors *UPC2* and *ECM22* was examined (Fig. 7*A*). Of the 20 *ERG* genes analyzed, the expression of *ERG1*, *ERG11*, *ERG28*, and *ERG2* was significantly induced in *the cab1*^{ts} mutant compared with WT at 1.8-, 2.5-, 4.6-, and 2.4-fold, respectively (Fig. 7*B*). The *ERG4* gene, a sterol reductase catalyzing the final step in ergosterol biosynthesis, was the only gene in the *ERG* biosynthesis pathway found to be down-regulated in the mutant, although not significantly. The expression of the transcriptional factors *UPC2* and *ECM22* was not significantly different between the WT and the *cab1*^{ts} mutant (Fig. 7*B*). As a control, no significant differences between the WT and *cab1*^{ts} strains could be detected in the expression levels of the housekeeping *ACT1* gene (Fig. 7*B*).

Discussion

In this study, we provide the first evidence that changes in pantothenate phosphorylation, catalyzed by the pantothenate kinase Cab1p, control the metabolism of ergosterol and susceptibility of yeast cells to antifungal drugs. The *CAB1* gene encodes the only pantothenate kinase in *S. cerevisiae* and is essential for cell viability. Other fungi, including all *Candida*

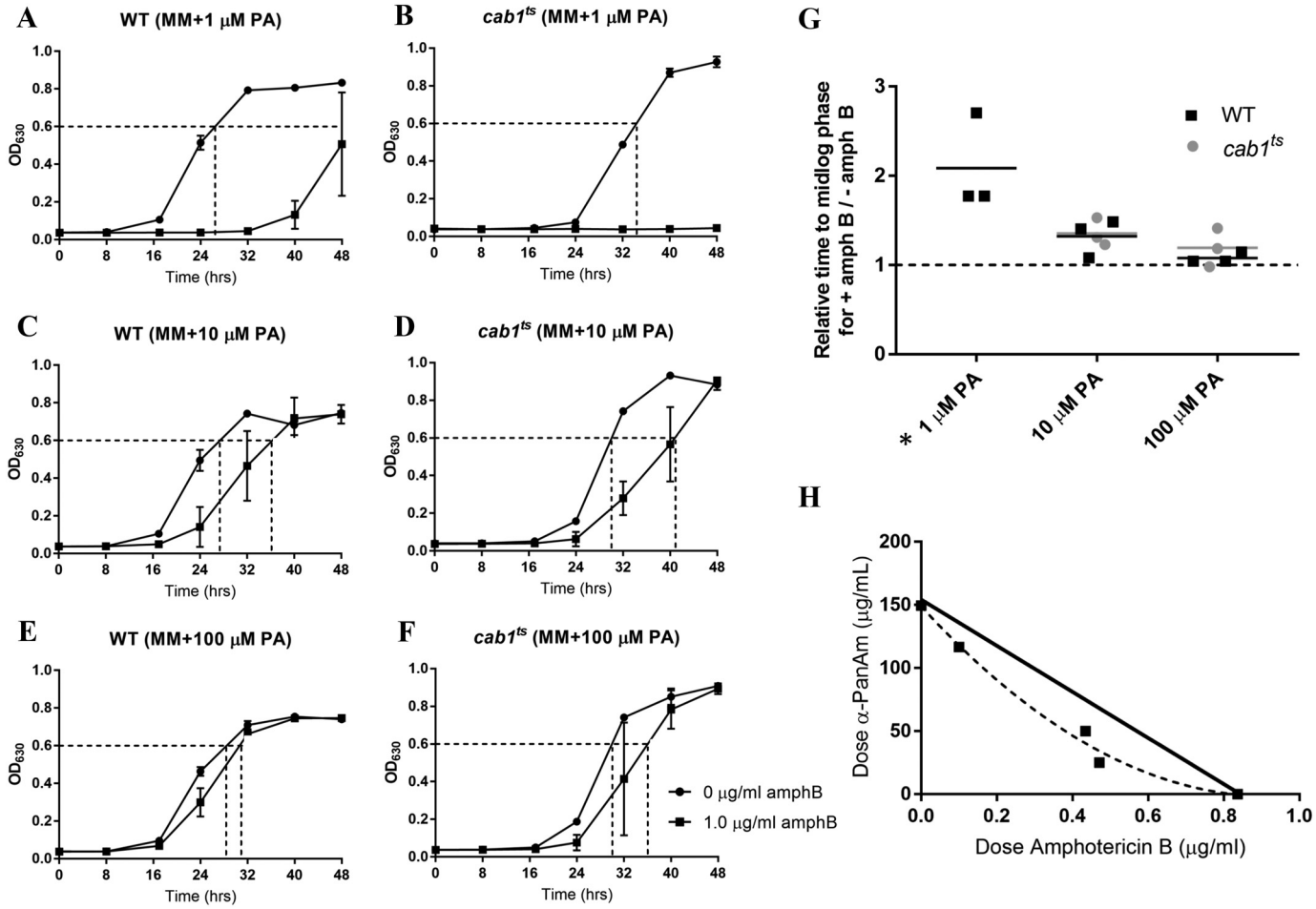

Figure 5. Relationship between pantothenate utilization and yeast susceptibility to amphotericin B. *A–F*, growth curves of WT and *cab1*^{ts} cells without or with 1 μg/ml amphotericin B (*amphB*) in liquid minimal medium supplemented with varying concentrations of pantothenic acid. *MM*, minimal medium. *G*, relative times for treated WT and *cab1*^{ts} cells to reach mid-log phase compared with untreated cells, calculated from *A*. Time for untreated cells to grow to mid-log was normalized to 1 and is represented by the *dashed line*. The *asterisk* (*) denotes that no relative times could be determined for the *cab1*^{ts} strain because the treated cells did not grow and never reached mid-log phase. *H*, isobologram of the interaction between amphotericin B and the pantothenate analog α-PanAm ($n = 2$). The *solid line* represents the theoretical curve of an additive effect. Data below the *solid line* (*dashed* curve) show synergism between the two compounds.

spp., *A. fumigatus*, *Cryptococcus neoformans*, and *Histoplasma capsulatum*, also express a single-copy gene encoding pantothenate kinase activity. Therefore, the encoded activity not only represents a promising new target in antifungal therapy but also a novel strategy to modulate the susceptibility of fungi to currently used antifungal drugs.

We took advantage of the availability of a thermosensitive *cab1*^{ts} strain, which expresses mutated Cab1p enzyme with a substitution of glycine 351 to serine, to examine the possible link between pantothenate utilization and both ergosterol metabolism and yeast susceptibility to antifungals. This amino acid substitution results in a dramatic decrease (>90%) in enzyme catalysis sufficient to allow cells to survive at 30 °C but not at 37 °C. Cell growth assays showed that at 30 °C the *cab1*^{ts} mutant is less susceptible to the antifungal drugs terbinafine, amorolfine, and fluconazole (all of which inhibit enzymes in late ergosterol biosynthesis) and more susceptible to amphotericin B (a drug that acts by forming 1:1 adducts with ergosterol rather than acting as an enzyme inhibitor) than the wild-type strain. The reduced sensitivity of the *cab1*^{ts} mutant to terbinafine was reversed in media supplemented with high concentrations of pantothenic acid. These data suggest that changes in the utilization of pantothenic acid to CoA through inhibition or activation of the pantothenate kinase modulate yeast sensitivity to antifungals that target ergosterol biosynthesis. This novel control mechanism was further investigated by mimicking the reduced pantothenate utilization activity of the *cab1*^{ts} strain by treating WT cells with the pantothenate analog α-PanAm (9). This compound was previously shown in both yeast cells and *Plasmodium falciparum* to inhibit CoA synthesis from pantothenic acid (9, 10). Consistent with the phenotype of the *cab1*^{ts} mutant, treatment of WT cells with α-PanAm resulted in decreased susceptibility to terbinafine and increased susceptibility to amphotericin.

To investigate the direct impact of pantothenate utilization on ergosterol metabolism, we compared sterol and gene expression levels between WT and *cab1*^{ts} strains. Of all sterols and precursors analyzed, squalene and ergosterol were the most predominant in both strains with significantly different levels detected in the *cab1*^{ts} mutant compared with the WT (Fig. 6). All other detected sterols, including lanosterol, T-MAS, fecosterol, lichesterol, episterol, ergosta-5,7-dien-3β-ol, and

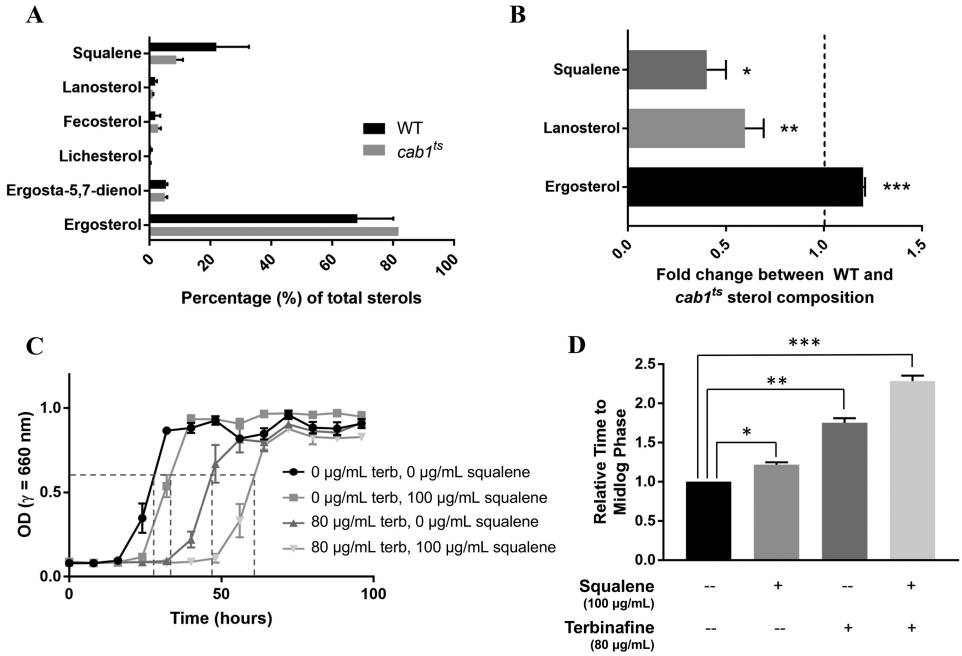

Figure 6. Effect of altered pantothenate phosphorylation on cellular sterol levels and sensitivity to terbinafine. *A*, the most prominent ergosterol precursors in the ergosterol biosynthetic pathway were chosen for analysis in both WT and *cab1*^{ts} cells. *B*, levels of squalene, lanosterol, and ergosterol in WT cells were normalized to 1 and are represented by the *dashed line* on the graph. *Bars* denote the -fold change in the relative level of each sterol in *cab1*^{ts} cells compared with WT. *, *p* value 0.0088; **, *p* value 0.0185; ***, *p* value 0.0009. *C*, growth of WT cells in defined liquid media with 100 μM PA supplemented with squalene, terbinafine (*terb*), or both ($n = 3$). *D*, relative times of treated cells to grow to mid-log phase compared with untreated cells, calculated from values in Fig. 6*C*. Untreated cells were normalized to 1. *, *p* value 0.0017; **, *p* value 0.0002; ***, *p* value < 0.0001. *Error bars* represent SD.

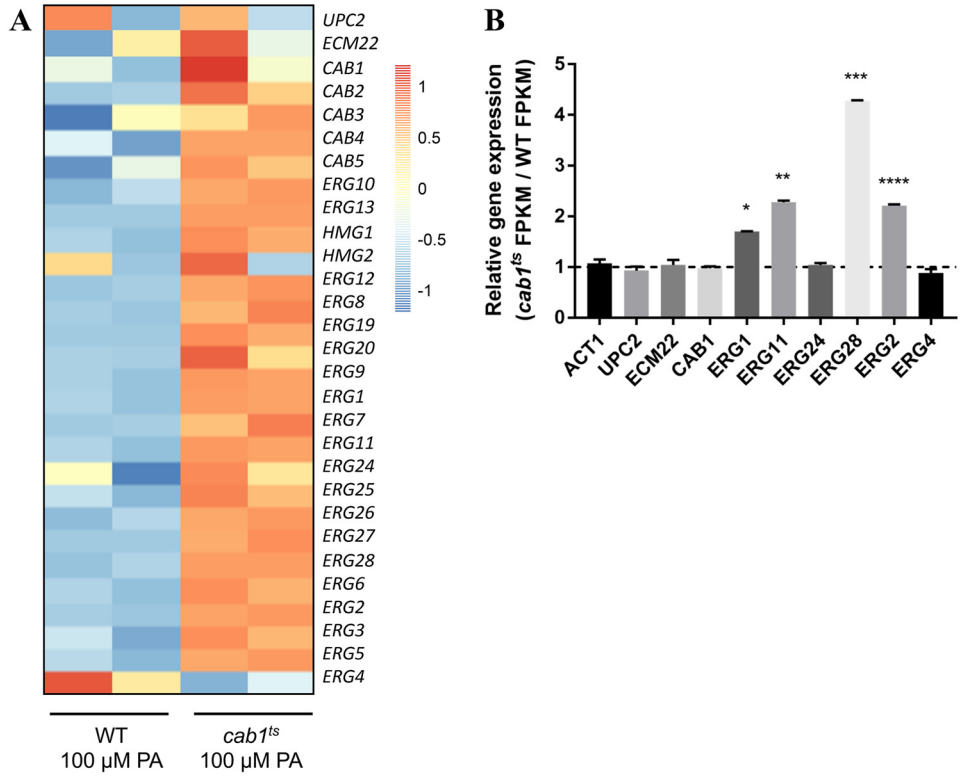

Figure 7. Effect of altered pantothenate phosphorylation on *CAB* and *ERG* gene transcription. *A*, heat map ($\log_2$ scale) showing changes in the expression levels of two transcription factors for the ergosterol biosynthesis pathway, *CAB* genes, and *ERG* genes between WT and *cab1*^{ts} cells grown in minimal media supplemented with 100 μM pantothenic acid. Two independent replicates of the WT strain are represented by the *left two columns*, and two replicates of the *cab1*^{ts} strain are represented by the *right two columns*. *B*, -fold change of gene expression levels (FPKM) between WT and *cab1*^{ts} strains ($n = 2$). For each gene, the level in the WT was set to 1 to normalize the data. The *bars* show relative -fold change of *cab1*^{ts} cells to WT for each gene. The relative FPKM levels of the *ACT1* gene are shown for control. *, *p* value 0.0011; **, *p* value 0.0013; ***, *p* value 0.0003; ****, *p* value < 0.0004. *Error bars* represent SD.

fungisterol, were present only in low quantities. Interestingly, the differences in squalene and ergosterol levels between the two strains were detected even though the cells were cultured in the presence of 100 μM pantothenic acid, which activates the metabolism of ergosterol and stimulates the growth of the *cab1^{ts}* to levels similar to those found in the WT strain. Equally interestingly, transcriptional analysis revealed that the expression levels of several *ERG* genes were increased in the *cab1^{ts}* mutant, including the *ERG1* gene involved in squalene epoxidation. This suggests that the low steady-state levels of squalene in the mutant are due to both reduced metabolic input from the CoA biosynthesis pathway and increased squalene utilization by Erg1p, leading to reduced accumulation of this intermediate in the presence of terbinafine and consequently reduced sensitivity to the drug. This was further demonstrated in our studies as the susceptibility of WT cells to terbinafine was found to increase dramatically in the presence of excess squalene (Fig. 6*C*).

Our studies have shown that, in addition to its reduced susceptibility to the squalene epoxidase inhibitor terbinafine, the *cab1^{ts}* mutant also displays reduced susceptibility to amorolfine and fluconazole. Whereas fluconazole targets the Erg11p enzyme (a cytochrome P450 enzyme), amorolfine targets both the Erg24p and Erg2p enzymes, catalyzing double bond modifications in the sterol backbone. Consistent with the reduced susceptibility of *cab1^{ts}* cells to amorolfine, the levels of lanosterol, the substrate of Erg11p, were significantly lower in the *cab1^{ts}* mutant compared with the WT, whereas the transcription of its encoding gene was increased. Additionally, we found that the transcription levels of *ERG24* and *ERG2* genes were significantly higher in the *cab1^{ts}* mutant than in the WT. Together, the data are consistent with the model that a reduced input from the CoA pathway into the ergosterol biosynthesis pathway and a concomitant increase in the expression of the *ERG* genes involved in both the mevalonate and distal ergosterol biosynthesis pathways result in reduced levels of toxic intermediates of ergosterol biosynthesis, which would otherwise accumulate upon enzyme inhibition by drug classes targeting the distal synthesis pathway. Conversely, the increased susceptibility of the *cab1^{ts}* strain to amphotericin B, which forms adducts with ergosterol on the membrane (9), was enhanced compared with the WT. Consistent with this finding, we analyzed the top 60 most-changed genes in global yeast transcription (Fig. S1). We found expression of *DAN1* and *DAN4*, which are involved in the storage of ergosterol (15), to be significantly increased in the *cab1^{ts}* mutant (Fig. S2*A*). Furthermore, expression of *ARE1*, *ARE2*, and *NPC2*, genes involved in the storage of sterols (16, 17), were also altered in the mutant (Fig. S2*B*). Significant up-regulation of *ARE2* was seen in the mutant, suggesting increased sterol esterification and storage in the endoplasmic reticulum. Additionally, significant down-regulation of *NPC2* was observed in *cab1^{ts}* (Fig. S2*B*), a genetic modulation that is typically associated with the phenotype of massive lysosomal accumulation of sterols (17). These data suggest that perhaps the *cab1^{ts}* mutant stores higher amounts of ergosterol in organelles, resulting in the higher ergosterol content observed in Fig. 6. The other major family of intracellular sterol-binding proteins, the *OSH* gene family, was also examined for changes in transcription. This family has previously been implicated in sterol transport between organelles (18). Data showed that the family was not systemically up- or down-regulated, although the transcription of *OSH5* was significantly reduced (Fig. S2*C*). Finally, transcription of genes associated with sterol export were studied, particularly the *PRY* gene family. Pry1p and Pry2p are secreted sterol-binding proteins, whereas Pry3p is cell wall–associated (19). *PRY3* was significantly down-regulated in *cab1^{ts}*, suggesting a possible decrease in the export of ergosterol in the mutant (Fig. S2*D*). In summary, available data suggest increased sterol uptake and storage and decreased sterol export in the *cab1^{ts}* mutant, which may account for its increased susceptibility to amphotericin B. Consistent with our proposed model for amphotericin B sensitivity of the *cab1^{ts}* mutant, studies by Hull *et al.* (20) showed that increased sterol uptake in *Candida glabrata* clinical isolates results in increased sensitivity to amphotericin B.

Altogether, our data suggest that pantothenate utilization controls ergosterol metabolism and the expression of *ERG* genes. Based on our model (Fig. 8), new strategies that exploit this mode of control by the pantothenate kinase may lead to better solutions for management of antifungal efficacy, toxicity, and resistance.

Experimental procedures

Yeast strains

S. cerevisiae strains used in this study were JS91.15-23 (WT: *MATα his3 leu2 trp1 ura3*) (8) and JS91.14-24 (*cab1^{ts}* mutant: *MATa ura3 his3 cab1^{ts}*) (8). WT and mutant strains were propagated either in YPD medium or defined pantothenic acid-free (minimal) medium composed of yeast nitrogen base (MP Biomedicals), supplemented with complete supplement mixture (MP Biomedicals) and all vitamins except pantothenic acid. Where indicated, media were supplemented with appropriate concentrations of pantothenic acid.

Growth assays on solid and liquid media

Spotting assays were performed as follows. Precultures of WT and *cab1^{ts}* yeast strains were prepared in YPD medium overnight at 30 °C. Cells were harvested, washed, and diluted to 10^8 cells in 500 μl of sterile water. Subsequent serial dilutions were made, and 5 μl of cell suspensions were spotted on YPD agar plates (square Petri dish with grid) lacking or supplemented with 10 ng/ml amorolfine, 1 μg/ml amphotericin B, 10 μg/ml fluconazole, or 10 μg/ml terbinafine to achieve 10^6, 10^5, 10^4, 10^3, 10^2, and 10^1 cells/spot. Plates were incubated at 30 or 37 °C and imaged every 24 h. For liquid assays in 96-well plate format, cells were precultured overnight in liquid YPD medium at 30 °C, washed three times in water, and diluted to achieve 10^4 cells/well in 150 μl of minimal medium supplemented with 1, 10, or 100 μM pantothenic acid and either lacking or supplemented with terbinafine (160 μg/ml). All plates were incubated at 30 °C. Optical density measurements were taken with a BioTek SynergyMx microplate reader (OD_{630}) every 8 h for a total of 96 h. Relative time to mid-log phase was calculated by first graphing growth curves and then determining the time at which each curve reached mid-log growth saturation, chosen to be an OD of 0.6.

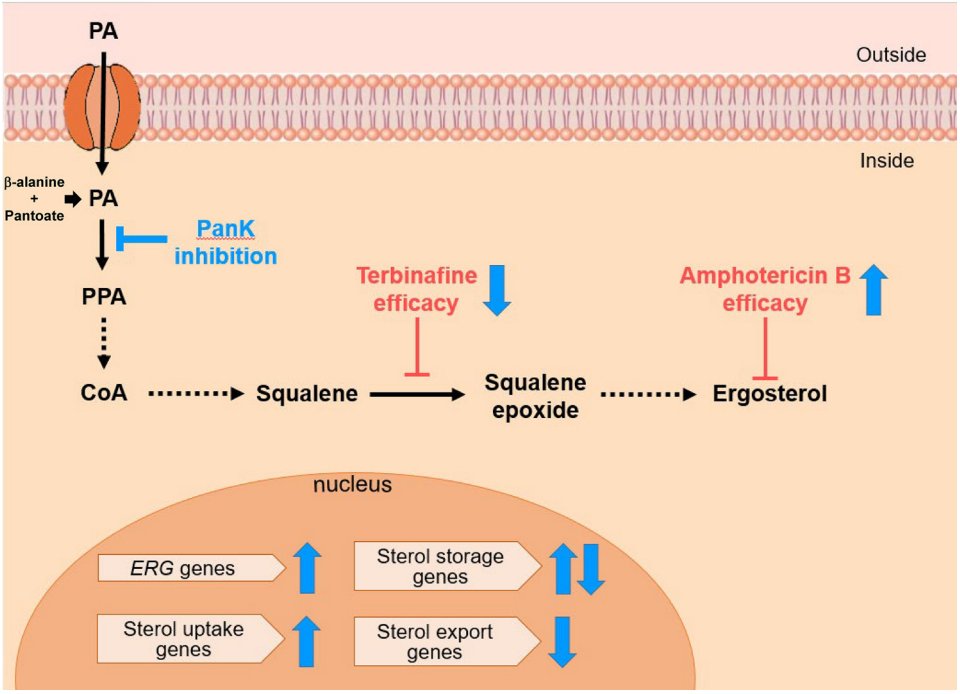

Figure 8. Model of the mode of control of ergosterol biosynthesis and sensitivity to antifungal by CoA biosynthesis pathway. Inhibition or reduction of Cab1p activity through genetic mutation (use of *cab1*^{ts} mutant strain) or enzyme inhibition (addition of α-PanAm) results in reduced sensitivity to terbinafine and increased sensitivity to amphotericin B. Conversely, activation of Cab1p through supplementation with exogenous pantothenate or a surrogate for Cab1p activation by the addition of squalene results in increased sensitivity to terbinafine and reduced sensitivity to amphotericin B. *PPA*, phosphopantothenate; *PanK*, pantothenate kinase.

Pantothenate kinase activity assay

The activity of recombinant His$_6$-tagged Cab1p and Cab1^{G351S}p was determined *in vitro* using the Kinase-Glo Plus Luminescent Kinase (Kinase-Glo) assay as described previously (9). The assay measures the amount of ATP remaining in solution following the kinase reaction. Briefly, kinase buffer consisted of 100 mM Tris-HCl, pH 7.4, 10 mM $MgCl_2$, 100 μM pantothenate (PA), 100 μM ATP, and 0.5 mg/ml γ-globulin. Kinase reactions were initiated with the addition of 500 ng of purified Cab1p or Cab1^{G351S}p in elution buffer (10 mM Tris, pH 7.4, NaCl 10 mM, and 500 mM imidazole). Heat-inactivated (20 min at 80 °C) Cab1p and Cab1^{G351S}p were used as controls. Samples were incubated at room temperature for 1 h. At the end of the incubation, an equal volume (10 μl) of Kinase-Glo reagent was added to each sample, the plates were further incubated for 5 min, and luminescence was recorded using a BioTek SynergyMx microplate reader (excitation wavelength, 485 nm; emission wavelength, 528 nm).

Drug–drug interactions and isobologram calculations

First, MIC_{50} values for amorolfine, amphotericin B, fluconazole, and terbinafine against WT and *cab1*^{ts} cells grown in YPD liquid medium were calculated by the Clinical and Laboratory Standards Institute standard method M27-A3. Next, terbinafine–α-PanAm and amphotericin B–α-PanAm interactions were determined using liquid growth assays in 96-well plates using the checkerboard method as described previously (21). The isobologram was produced by solving for the sum 50% fractional inhibitory concentration ($\sum FIC_{50}$) using the following equation where previously calculated MIC_{50} values were used in the calculations.

$$\Sigma FIC_{50} = \frac{MIC_{50} \text{ of the drug combination}}{MIC_{50} \text{ of drug A alone}} + \frac{MIC_{50} \text{ of the drug combination}}{MIC_{50} \text{ of drug B alone}} \quad \text{(Eq. 1)}$$

The $\sum FIC_{50}$ values calculated here were used to generate the isobologram curves.

Sterol analysis

Four independent 25-ml cultures of WT and *cab1*^{ts} were prepared in minimal medium supplemented with 100 μM PA at a starting cell density of 10^4 cells/ml and incubated at 30 °C until they reached mid-log phase (average OD_{630} ~0.6). Cells were then washed once in PBS, weighed, and stored at −80 °C until used. The sterol pattern was determined by GC-MS as described previously (22, 23). The quantification, managed with an external calibration with ergosterol for the detected sterols and squalene for the content of squalene, consists of six levels with concentrations up to 10 μg/ml. The base peak of each sterol trimethylsilyl ether (squalene and cholestane excluded) were taken as a quantifier ion for calculating the peak areas for squalene *m*/*z* 69, internal standard cholestane *m*/*z* 217, lichesterol (ergosta-5,8,22-trien-3β-ol) *m*/*z* 363, ergosterol (ergosta-5,7,22-trien-3β-ol) *m*/*z* 363, ergosta-5,7-dien-3β-ol *m*/*z* 365, fecosterol (ergosta-7,24(28)-dien-3β-ol) *m*/*z* 343, episterol (ergosta-7,24(28)-dien-3β-ol) *m*/*z* 343, fungisterol (ergost-7-en-3β-ol) *m*/*z* 472, lanosterol (4,4,14-trimethylcholesta-8,24-dien-3β-ol) *m*/*z* 393, and T-MAS (4,4-dimethylcholesta-8,24-dien-3β-ol) *m*/*z* 379.

Transcriptomic analysis

RNA-Seq was performed to compare the transcriptional profiles of the WT and the *cab1^{ts}* strains grown in minimal medium with 100 μM pantothenic acid (conditions at which the strains showed equal growth). RNA was isolated from cultures of WT and *cab1^{ts}* strains using the RiboPure^{TM} RNA Purification kit (Invitrogen), and RNA-Seq was performed by running the samples on a HiSeq2500 in high-output mode 1 × 75 (200 million reads/lane). The reads were trimmed for quality and aligned with the hg19 reference genome using TopHat2 (24). The transcripts were assembled using Cufflinks (25). The assembled transcripts were used to estimate transcript abundance and differential gene expression using the Cuffdiff program (25). The results were visualized using R (CRAN) and CummeRbund (26).

Statistics

Relative times to mid-log phase of *cab1^{ts}* cells compared with WT cells in liquid media with terbinafine or amphotericin B treatment were analyzed by unpaired *t* tests with α value 0.05, resulting in two-tailed *p* values. For relative time to mid-log phase in 160 μg/ml terbinafine and 1 μM PA: *p* value <0.0001, *t* value = 23.52, *df* = 4, *n* = 3; 160 μg/ml terbinafine and 10 μM PA: *p* value <0.0001, *t* value = 43.43, *df* = 4, *n* = 3; and 160 μg/ml terbinafine and 100 μM PA: *p* value <0.0001, *t* value = 54.73, *df* = 4, *n* = 3. For relative time to mid-log phase in 1 μg/ml amphotericin B and 10 μM PA: *p* value = 0.8034, *t* value = 0.2386, *df* = 2, *n* = 3; 1 μg/ml amphotericin B and 100 μM PA: *p* value = 0.3505, *t* value = 1.208, *df* = 2, *n* = 3.

-Fold changes of the sterols squalene, lanosterol, and ergosterol were analyzed by paired *t* tests with α value 0.05, resulting in two-tailed *p* values. For -fold change squalene *versus* WT, *p* value = 0.0088, *t* value = 10.61, *df* = 2, *n* = 3. For -fold change lanosterol *versus* WT, *p* value = 0.0185, *t* value = 7.253, *df* = 2, *n* = 3. For -fold change ergosterol *versus* WT, *p* value = 0.0009, *t* value = 33.22, *df* = 2, *n* = 3.

Relative time of growth in liquid media for WT cells treated with squalene and/or terbinafine compared with untreated WT cells was analyzed by unpaired *t* tests with α value 0.05, resulting in two-tailed *p* values. For cells treated with 100 μg/ml squalene, 0 μg/ml terbinafine, *p* value = 0.0017, *t* value = 7.493, *df* = 4, *n* = 3. For cells treated with 0 μg/ml squalene, 80 μg/ml terbinafine, *p* value = 0.0002, *t* value = 12.64, *df* = 4, *n* = 3. For cells treated with 100 μg/ml squalene, 80 μg/ml terbinafine, *p* value<0.0001, *t* value = 52.56, *df* = 4, *n* = 3.

Comparison of RNA transcript levels in the form of FPKM values between WT and *cab1^{ts}* cells was statistically analyzed by unpaired *t* tests with α value 0.05, resulting in two-tailed *p* values. The following results were obtained: *ACT1*: *p* value = 0.1823, *t* value = 2.009, *df* = 2, *n* = 2; *UPC2*: *p* value = 0.9826, *t* value = 0.024, *df* = 2, *n* = 2; *ECM22*: *p* value = 0.4907, *t* value = 0.837, *df* = 2, *n* = 2; *CAB1*: *p* value = 0.2669, *t* value = 1.524, *df* = 2, *n* = 2; *ERG1*: *p* value = 0.0011, *t* value = 29.99, *df* = 2, *n* = 2; *ERG11*: *p* value = 0.0013, *t* value = 28.21, *df* = 2, *n* = 2; *ERG24*: *p* value = 0.1965, *t* value = 1.909, *df* = 2, *n* = 2; *ERG28*: *p* value = 0.0003, *t* value = 54.77, *df* = 2, *n* = 2; *ERG2*: *p* value = 0.0004, *t* value = 47.94, *df* = 2, *n* = 2; *ERG4*: *p* value = 0.1103, *t* value = 2.755, *df* = 2, *n* = 2; *DAN1*: *p* value = 0.0198, *t* value = 7.008, *df* = 2, *n* = 2; *DAN4*: *p* value = 0.0052, *t* value = 13.78, *df* = 2, *n* = 2; *AUS1*: *p* value = 0.3317, *t* value = 1.27, *df* = 2, *n* = 2; *PDR11*: *p* value = 0.2838, *t* value = 1.451, *df* = 2, *n* = 2; *SUT1*: *p* value = 0.8514, *t* value = 0.2125, *df* = 2, *n* = 2; *ARE1*: *p* value = 0.0266, *t* value = 6.014, *df* = 2, *n* = 2; *ARE2*: *p* value = 0.0189, *t* value = 7.17, *df* = 2, *n* = 2; *NPC2*: *p* value = 0.0482, *t* value = 4.388, *df* = 2, *n* = 2; *YFT2*: *p* value = 0.0609, *t* value = 3.866, *df* = 2, *n* = 2; *OSH7*: *p* value = 0.1107, *t* value = 2.75, *df* = 2, *n* = 2; *OSH1/SWH1*: *p* value = 0.3304, *t* value = 1.275, *df* = 2, *n* = 2; *OSH2*: *p* value = 0.1786, *t* value = 2.037, *df* = 2, *n* = 2; *OSH3*: *p* value = 0.4847, *t* value = 0.8503, *df* = 2, *n* = 2; *OSH4/KES1*: *p* value = 0.0669, *t* value = 3.67, *df* = 2, *n* = 2; *OSH5/HES1*: *p* value = 0.0195, *t* value = 7.063, *df* = 2, *n* = 2; *OSH6*: *p* value = 0.6636, *t* value = 0.5053, *df* = 2, *n* = 2; *PRY1*: *p* value = 0.071, *t* value = 3.536, *df* = 2, *n* = 2; *PRY2*: *p* value = 0.0604, *t* value = 3.882, *df* = 2, *n* = 2; *PRY3*: *p* value = 0.0085, *t* value = 10.76, *df* = 2, *n* = 2.

Author contributions—J. E. C., S. M., and C. M. formal analysis; J. E. C., J. T., and C. M. investigation; J. E. C. and C. B. M. visualization; J. E. C., J. T., C. M., and F. B. methodology; J. E. C., J. T., C. M., F. B., and C. B. M. writing-original draft; J. T., C. M., and F. B. resources; S. M. and F. B. data curation; C. B. M. conceptualization; C. B. M. supervision; C. B. M. project administration.

Acknowledgments—We thank Dr. Hans-Joachim Schüller for providing strains JS91.15-23 and JS91.14-24 used in this study. We thank Christopher Castaldi, Shrikant Mane, and Guilin Wang at the Yale Genome Center for assistance with RNA-Seq analysis; Benjamin Perrin for assistance with drug assays; and Dr. Theodore C. White for valuable comments.

References

1. Soni, P., Parihar, R. S., and Soni, L. K. (2017) Opportunistic microorganisms in oral cavity according to treatment status in head and neck cancer patients. *J. Clin. Diagn Res.* **11,** DC14–DC17 CrossRef Medline
2. Williams, C., Ranjendran, R., and Ramage, G. (2016) Pathogenesis of fungal infections in cystic fibrosis. *Curr. Fungal Infect. Rep.* **10,** 163–169 CrossRef Medline
3. Brown, G. D., Denning, D. W., Gow, N. A., Levitz, S. M., Netea, M. G., and White, T. C. (2012) Hidden killers: human fungal infections. *Sci. Transl. Med.* **4,** 165rv13 CrossRef Medline
4. Vanden, B. H., Dromer, F., Improvisi, I., Lozano-Chiu, M., Rex, J., and Sanglard, D. (1998) Antifungal drug resistance in pathogenic fungi. *Med. Mycol.* **36,** Suppl. 1, 119–128 Medline
5. Gout, I. (2018) Coenzyme A, protein CoAlation and redox regulation in mammalian cells. *Biochem. Soc. Trans.* **46,** 721–728 CrossRef Medline
6. Stolz, J., and Sauer, N. (1999) The fenpropimorph resistance gene FEN2 from *Saccharomyces cerevisiae* encodes a plasma membrane H^+-pantothenate symporter. *J. Biol. Chem.* **274,** 18747–18752 CrossRef Medline
7. Marcireau, C., Joets, J., Pousset, D., Guilloton, M., and Karst, F. (1996) FEN2: a gene implicated in the catabolite repression-mediated regulation of ergosterol biosynthesis in yeast. *Yeast* **12,** 531–539 CrossRef Medline
8. Olzhausen, J., Schübbe, S., and Schüller, H. J. (2009) Genetic analysis of coenzyme A biosynthesis in the yeast *Saccharomyces cerevisiae*: identification of a conditional mutation in the pantothenate kinase gene CAB1. *Curr. Genet.* **55,** 163–173 CrossRef Medline
9. Chiu, J. E., Thekkiniath, J., Choi, J. Y., Perrin, B. A., Lawres, L., Plummer, M., Virji, A. Z., Abraham, A., Toh, J. Y., Zandt, M. V., Aly, A. S. I., Voelker, D. R., and Mamoun, C. B. (2017) The antimalarial activity of the pantothenamide α-PanAm is via inhibition of pantothenate phosphorylation. *Sci. Rep.* **7,** 14234 CrossRef Medline

10. de Villiers, M., Spry, C., Macuamule, C. J., Barnard, L., Wells, G., Saliba, K. J., and Strauss, E. (2017) Antiplasmodial mode of action of pantothenamides: pantothenate kinase serves as a metabolic activator not as a target. *ACS Infect. Dis.* **3,** 527–541 CrossRef Medline
11. Bhattacharya, S., Esquivel, B. D., and White, T. C. (2018) Overexpression or deletion of ergosterol biosynthesis genes alters doubling time, response to stress agents, and drug susceptibility in *Saccharomyces cerevisiae*. *MBio* **9,** e01291-18 Medline
12. Ryder, N. S. (1992) Terbinafine: mode of action and properties of the squalene epoxidase inhibition. *Br. J. Dermatol.* **126,** 2–7 CrossRef Medline
13. Carrillo-Muñoz, A., Giusiano, G., Ezkurra, P. A., and Quindós, G. (2006) Antifungal agents: mode of action in yeast cells. *Rev. Esp. Quimioter.* **19,** 130–139 Medline
14. Ryder, N. (1986) Biochemical mode of action of the allylamine antimycotic agents naftifine and SF 86-327, *In Vitro and in Vivo Evaluation of Antifungal Agents* (Iwata, K., and Vanden Bossche, H., eds) pp. 88–99, Elsevier Science Publishers BV, Amsterdam
15. South, P. F., Harmeyer, K. M., Serratore, N. D., and Briggs, S. D. (2013) H3K4 methyltransferase Set1 is involved in maintenance of ergosterol homeostasis and resistance to brefeldin A. *Proc. Natl. Acad. Sci. U.S.A.* **110,** E1016–E1025 CrossRef Medline
16. Tian, S., Ohta, A., Horiuchi, H., and Fukuda, R. (2015) Evaluation of sterol transport from the endoplasmic reticulum to mitochondria using mitochondrially targeted bacterial sterol acyltransferase in *Saccharomyces cerevisiae*. *Biosci. Biotechnol. Biochem.* **79,** 1608–1614 CrossRef Medline
17. Pfeffer, S. R. (2019) NPC intracellular cholesterol transporter 1 (NPC1)-mediated cholesterol export from lysosomes. *J. Biol. Chem.* **294,** 1706–1709 CrossRef Medline
18. Tian, S., Ohta, A., Horiuchi, H., and Fukuda, R. (2018) Oxysterol-binding protein homologs mediate sterol transport from the endoplasmic reticulum to mitochondria in yeast. *J. Biol. Chem.* **293,** 5636–5648 CrossRef Medline
19. Choudhary, V., and Schneiter, R. (2012) Pathogen-related yeast (PRY) proteins and members of the CAP superfamily are secreted sterol-binding proteins. *Proc. Natl. Acad. Sci. U.S.A.* **109,** 16882–16887 CrossRef Medline
20. Hull, C. M., Parker, J. E., Bader, O., Weig, M., Gross, U., Warrilow, A. G., Kelly, D. E., and Kelly, S. L. (2012) Facultative sterol uptake in an ergosterol-deficient clinical isolate of *Candida glabrata* harboring a missense mutation in ERG11 and exhibiting cross-resistance to azoles and amphotericin B. *Antimicrob. Agents Chemother.* **56,** 4223–4232 CrossRef Medline
21. Orhan, G., Bayram, A., Zer, Y., and Balci, I. (2005) Synergy tests by E test and checkerboard methods of antimicrobial combinations against *Brucella melitensis*. *J. Clin. Microbiol.* **43,** 140–143 CrossRef Medline
22. Müller, C., Neugebauer, T., Zill, P., Lass-Flörl, C., Bracher, F., and Binder, U. (2018) Sterol composition of clinically relevant Mucorales and changes resulting from posaconazole treatment. *Molecules* **23,** E1218 CrossRef Medline
23. Muller, C., Binder, U., Bracher, F., and Giera, M. (2017) Antifungal drug testing by combining minimal inhibitory concentration testing with target identification by gas chromatography-mass spectrometry. *Nat. Protoc.* **12,** 947–963 CrossRef Medline
24. Trapnell, C., Pachter, L., and Salzberg, S. L. (2009) TopHat: discovering splice junctions with RNA-Seq. *Bioinformatics* **25,** 1105–1111 CrossRef Medline
25. Trapnell, C., Hendrickson, D. G., Sauvageau, M., Goff, L., Rinn, J. L., and Pachter, L. (2013) Differential analysis of gene regulation at transcript resolution with RNA-seq. *Nat. Biotechnol.* **31,** 46–53 CrossRef Medline
26. Trapnell, C., Roberts, A., Goff, L., Pertea, G., Kim, D., Kelley, D. R., Pimentel, H., Salzberg, S. L., Rinn, J. L., and Pachter, L. (2012) Differential gene and transcript expression analysis of RNA-seq experiments with TopHat and Cufflinks. *Nat. Protoc.* **7,** 562–578 CrossRef Medline